# The 1988-2003 Greenland ice sheet melt extent using passive microwave satellite data and a regional climate model

Xavier Fettweis[1], Hubert Gallée[2], Filip Lefebre[3], Jean-Pascal van Ypersele[1]

**Abstract.** Measurements from ETH-Camp and JAR1 AWS (West Greenland) as well as coupled atmosphere-snow regional climate simulations have highlighted flaws in the cross-polarized gradient ratio (XPGR) technique used to identify melt from passive microwave satellite data. It was found that dense clouds (causing notably rainfall) on the ice sheet severely perturb the XPGR melt signal. Therefore, the original XPGR melt detection algorithm has been adapted to better incorporate atmospheric variability over the ice sheet and an updated melt trend for the 1988-2003 period has been calculated. Compared to the original algorithm, the melt zone area increase is eight times higher (from 0.2 to 1.7 % $yr^{-1}$). The increase is higher with the improved XPGR technique because rainfall also increased during this period. It is correlated to higher atmospheric temperatures. Finally, the model shows that the total ice sheet runoff is directly proportional to the melt extent surface detected by satellites. These results are important for the understanding of the effect of Greenland melting on the stability of the thermohaline circulation.

[1] *Institut d'astronomie et de géophysique de G. Lemaître, Université catholique de Louvain, 2, chemin du cyclotron, B-1348 Louvain-La-Neuve, Belgium.*
[2] *Laboratoire de Glaciologie et Géophysique de l'Environnement, CNRS, Grenoble, France.*
[3] *Vito-IMS (Flemish Institute for Technological Research - Integral Environmental Studies) Mol, Belgium.*

*Author: Tel: 0032 10 47 33 02, Fax: 0032 10 47 47 22, Email: fettweis@astr.ucl.ac.be*

# 1. Introduction

[1] Understanding and estimating how the surface melting regimes of the Greenland ice sheet respond to climate variability and change becomes increasingly important, to accurately evaluate the impact of modified meltwater fluxes on the thermohaline circulation. Remote sensing has an enormous potential to monitor melt on the Greenland ice sheet. Microwave data is particularly suited because it is not obstructed by clouds. Abdalati and Steffen (1997, 2001) developed the cross-polarized gradient ratio (XPGR) method to study interannual melt extent variations.

[2] We present here an intercomparison between the Greenland melt extent simulated by a regional climate model and the one derived from satellite data with the XPGR method. The model used is the MAR regional climate model (RCM) which will be briefly described in section 2. The MAR has been extensively validated over Greenland in 1990-1991 with in-situ measurements (Lefebre et al, 2003; Lefebre et al., 2005) and satellite derived data (Fettweis et al., 2005). The passive microwave satellite data come from the Special Sensor Microwave/Imager (SSM/I) which has been operational since July 1987. They are available at a resolution of 25 km, equal to the MAR's resolution. Section 3 presents the XPGR technique from Abdalati and Steffen (1997) used to retrieve the melt. The comparison with the melt extent simulated by MAR highlights inadequacies in XPGR during rainfall events on the ice sheet (due to the presence of dense clouds). Improvements to the XPGR algorithm are presented in section 4. A high correlation was found between MAR simulated runoff and satellite derived melt extent. In section 5, this allows us to deduce the total ice sheet runoff from the melt extent detected by satellite. Finally, updated trends of a melt extent increase are shown in section 6.

# 2. MAR description

[3] The model used here is the RCM MAR (Modèle Atmosphérique Régional) coupled to the SISVAT (Soil Ice Snow Vegetation Atmosphere Transfer) scheme. The atmospheric part of MAR is fully described in Gallée and Schayes (1994), while the SISVAT scheme is detailed in De Ridder and Gallée (1998) and in Gallée et al. (2001). The simulation starts in September 1989 and lasts till September 2002 with a resolution of 25 km. We have used the ECMWF ERA-40 reanalysis to initialize the meteorological fields on 1 September 1989 and to force the MAR lateral boundaries every 6 hours. The

schemes and the setup used here are fully described in Fettweis et al. (2005) that used the first two years of this simulation.

---

# 3. Passive microwave satellite data

## 3.1. Data

[4] The brightness temperatures used for the remote sensing melt monitoring come respectively from the SSM/I F-8 satellite (1987-1991), the SSM/I F-11 satellite (1992-1994) and the SSM/I F-13 satellite (1995-2003). These data are provided by the National Snow and Ice Data Center (NSIDC, Boulder, Colorado). They are arranged on a regular grid of 25 km x 25 km and are available twice a day (Armstrong et al., 1994). Before interpolating these data to the model grid, we have averaged both of the satellite passages per day as Abdalati and Steffen (1997 and 2001) (noted respectively AS1997 and AS2001). Missing data have been corrected through linear interpolation in time if the gaps were shorter than three days as in Torinesi et al. (2003).

## 3.2. XPGR method

[5] The approach of AS1997 is used here to deduce the melt extent over the ice sheet from the satellite data. This technique has been developed for the Greenland ice sheet by comparison with in-situ observations in the snow pack and uses multiple frequencies and polarizations to take advantage of their differing responses to the Liquid Water Content (LWC) increase inside the snow pack. When this method detects melt, it gives the LWC of the snow pack which is very useful to compare with a model. Another algorithm has recently been developed by Torinesi et al. (2003) using only the 19-Ghz horizontal polarized brightness temperature. But i) this technique has been calibrated/validated only in Antarctica, ii) it detects mainly the surface melt and not the massive melt as observed in Greenland and iii) it does not give the LWC equivalent of the snow pack. For these reasons, we use the AS1997 retrieval melt algorithm.

[6] The AS1997 method is based on the cross-polarized gradient ratio (XPGR), which is defined as the normalized difference between the 19-GHz horizontal polarized brightness temperature (T19H) and the 37-GHz vertical polarized brightness temperature (T37V):

$$XPGR = \frac{T_b(19\mathrm{H}) - T_b(37\mathrm{V})}{T_b(19\mathrm{H}) + T_b(37\mathrm{V})} \quad [1]$$

A XPGR threshold value is then used to distinguish melt from non-melt points. The threshold values were determined by comparing XPGR to LWC of the snow pack at
93 ETH-Camp (Greenland) and by intercalibration between the different data sets. The XPGR threshold was determined by AS2001 to be -0.0158 for both SSM/I F-8 and F-11 satellites and -0.0154 for the SSM/I F-13 data. The SSM/I F-11 brightness temperatures
96 need to be intercalibrated to the F-8 baseline before using these thresholds (AS2001). When XPGR detects melt, it corresponds approximately to a LWC of 1 % by volume in the top metre of snow (AS1997). We use this last criterion to distinguish melt in the
99 MAR simulation. According to AS1997, bare ice (i.e. when the winter snow pack has completely melted and the ice appears) in the ablation zone is assumed to be melting in the model.

---

# 102 4. Modelled and satellite observed melt extent

## 4.1. Improving the original XPGR method

[7] Fettweis et al. (2005) found that the MAR simulated extent and time evolution of
105 the wet snow zone compare very well with the XPGR derived estimates during the 1990 and 1991 melt seasons. During rainfall events on the ice sheet, the satellite retrieved melt was however found to be underestimated by XPGR. The 19-GHz channel is known
108 be not very sensitive to the atmospheric variability (AS1997) but, the wavelengh of the 37-GHz channel is of the order of the diameter of water droplets in the clouds which contaminates the signal emitted by the surface.

111 [8] This bias can be seen in 1991 at ETH-Camp, located some 40 km away from the ice-sheet margin, close to the long-term equilibrium line, at 1154 m a.s.l.. XPGR detects melt when the LWC is above 1% by volume in the top metre of snow. Figure 1 plots
114 here the LWC of the observed snow pack above the ice (Ohmura et al., 1992). The LWC reaches values above 1% during the whole period shown in Figure 1, except in mid-June although XPGR detects melt. During this period, the height of the observed snow pack
117 is about 1.4 m and the LWC of the top metre of snow is higher than the LWC of the total snow pack because the melt water has not yet reached the depths of the snow pack at the beginning of the melt season. That is why XPGR detects melt during this event.
120 At the end of August, although the 2m-temperature is below zero degrees, the snow pack is still detected as melting by XPGR because the freezing surface temperatures are not low enough to refreeze the liquid melt water from deeper area. However, XPGR

fails several times to detect melt because the T37V is too warm, while the LWC of the snow pack is above 1% and the 2m-temperature is above the freezing point. Rainfall was observed at ETH-Camp in most of these cases which suggests perturbations in the remote observed melt signal.

# Figure 1

[9] Some abnormal short gaps in the melt season detected by XPGR can also be seen in Figure 2 at the JAR1 automatic weather station (AWS) from the Greenland Climate Network (GC-Net). This AWS is situated underneath ETH-Camp at 962 m a.s.l. in the ablation zone. During the warm 1998 summer, the snow pack was observed to melt about 2.4 m of water equivalent, continuously from May 24$^{th}$ until the end of September (Steffen et al., 2001). XPGR fails several times to detect melt during some days in the melt season when i) it detects melt some days before/after the day considered and ii) the observed (and simulated) 2m-temperature remains positive during each of these small episodes. Therefore the snow pack should continue to be detected as melting during these days as it was observed on the site (Steffen et al., 2001). For almost each of them, low shortwave incoming radiative fluxes were measured at JAR1 indicating dense clouds, and rainfall was simulated by MAR most of the time. A rainfall/snowfall episode at the end of May postpones the melt onset to the 28$^{th}$ of May in XPGR fields. After September 7$^{th}$ the snow pack begins to refreeze from the surface due to lower air temperatures, but the snow pack is still detected as melting because of the deeper liquid melt water. The improved XPGR algorithm (see below) and MAR detect successfully melt continuously from May 22$^{th}$ to the end of September (not shown here). Finally, a good agreement between the measured and modelled 2m-temperature was highlighted in Figure 2.

# Figure 2

[10] The perturbations, as discussed in the paragraph before, are largely due to dense clouds in the XPGR melt signal. This is also highlighted in Figures 3 and 4 where abnormal low melt signals detected by XPGR are mostly associated to rainfall events simulated by MAR. Hence the XPGR algorithm must be improved to better incorporate the atmospheric variability. During rainfall events notably, XPGR does not detect melt most of the time because T37V is abnormally high. The ideal solution would be to correct

T37V but it is difficult to detect efficiently the perturbations due to atmospheric variability. Therefore, we propose four different improvements to the XPGR algorithm. The original XPGR melt retrieval algorithm from AS1997 together with these fours improvements is denoted hereafter ImpXPGR.

i) We impose the continuity of the melt season to remove gaps shorter than three days between two melting days. The XPGR method is aimed to detect massive melt i.e. when the LWC is higher than 1% in the top metre of snow. Therefore short gaps in the middle of the melt season detected by XPGR, as those shown at ETH-Camp and at JAR1 AWS, are mostly unrealistic. They are in general found to be associated with dense clouds mostly causing precipitation on the ice sheet. It is clear that the snow pack continues to melt when it is raining. When it is snowing, the fresh snow layer above the melting snow pack is normally insufficient to decrease the LWC below 1 % in the top metre of snow. In the middle of the summer, a snow pack with a LWC of 2 % and more is usual and therefore more than 50 cm of fresh snow is needed so that the pixel is not detected as melting any more. Rather than dry fresh snow addition, lower temperatures that refreeze the melt water deeper in the snow pack can efficiently mask the melt signal. However, as shown at ETH-Camp and at JAR1 AWS, periods of refreeze during the melt season lasting less than three days are too short to refreeze in depth the liquid melt water which prolongs the remote detection of the melt (AS1997). XPGR without corrections detects successfully melt during these refreeze events. The satellites stops to detect melt at the end of the ablation season until the subsurface snow has refrozen. This correction constitutes the main improvement as shown both in Figures 4g and 5.

ii) Pixels situated at lower altitudes than three adjacent pixels where XPGR detects melt are classified as melting pixels. Indeed, the true resolution of T19H is 69 x 43 $km^2$ and 37 x 28 $km^2$ for T37V. These values are then interpolated on a regular grid (25 km x 25 km) by the NSIDC. Therefore, the signal emitted by the ice sheet margin pixels near sea, fjord or fresh melt water lake, in the tundra or on the ice sheet are contaminated by the water signal which is very different from the snow/ice signal. This second correction allows to resolve this problem to a large extent. Nevertheless, the intersection of both MAR and AS1997 ice sheet mask (removing a part of MAR ice sheet margin pixels) is used in both Figures 3 and 4 for a better comparison between XPGR and the improved XPGR.

iii) For each year, we compute the mean T19H temperature and the standard deviation over time and over all the grids points where XPGR (+ corrections i) and ii)) detects melt. We add half of the mean standard deviation to this average. This computed value is spatially constant and varies only interannually around 235K to take into account differences between the three satellites of SSM/I data as the XPGR threshold. If T19H is above this value, we assume that melt takes place. On the one hand, to remove eventual anomalies in SSM/I brightness temperature fields. On the other hand, to detect melt along the ice sheet margin. It is a correction à la Torinesi et al (2003). The 19-GHz channel is chosen because it is the least sensitive to the atmospheric variability. As for the second improvement, this correction improves the remote melt detection along the ice sheet margin (see Figure 5).

iv) As for the third improvement, we compute the mean T19H temperature and the standard deviation but now when XPGR does not detect melt. We subtract half of the mean standard deviation from this average. To remove anomalies in remote sensing observation, "no melt" is imposed if T19H is lower than this value (around 176 K). The third improvement adds melting pixels to the melt detected by the original XPGR at the beginning of the ablation season whereas the fourth improvement removes rather melting pixels at the end of the ablation season (See Figure 4g).

**Figure 3,4 & 5**

## 4.2. Comparison

[11] The agreement between the MAR simulated and the satellite retrieved melt becomes significantly better (Figures 3, 4 and 6) when ImpXPGR is used. The statistics are summarised in Table 1. MAR compares better with XPGR when rainfall/snowfall pixels are removed according to Fettweis et al. (2005). The removal of rainfall pixels does not improve the comparison with ImpXPGR because this last corrects the melt detection during rainfall. When snowfall pixels are removed, the agreement with ImpXPGR is better but the number of pixels taken into account in the comparison is significantly reduced. The yearly RMSE are shown in Figures 3 and 4 below each plot. The abnormally low satellite derived melt signal due to rainfall events are now corrected in a large part. See for example in Figures 3 and 4 the improvements during the following time periods: July 22-27$^{th}$ 1990, June 27-30$^{th}$ 1991, August 23-24$^{th}$ 1993, July 11-12$^{th}$ 1995, September 9-11$^{th}$ 1996, August 3$^{th}$ 1999, July 28-29$^{th}$ 2000, and multiple episodes

during the melt record years 1998 and 2002. The maximum melt extent area in July 2002 (Steffen et al. , 2004) is well simulated. The minimum occurs in summer 1992 due to the eruption of Mount Pinatubo (AS2001). The rainfall perturbations in the XPGR signal become insignificant at the end of melt season when the melt signal is then emitted only by sub-surface melt water (see both last plots of Figure 4). When the surface begins to refreeze, the melt signal comes mainly from the T19H channel which is less sensitive to the cloud liquid water contrary to the T37V channel.

[12] Both MAR and ImpXPGR detect much more melt than XPGR along the ice sheet margins (Figure 6). Indeed, the closer a pixel is to the ice sheet margin, the higher the probability to have rainfall or clouds with liquid water and the higher the probability that XPGR is biased. As already pointed out by Fettweis et al. (2005), MAR simulates less melt along the eastern and south-eastern mountainous regions of the ice sheet than the XPGR and the ImpXPGR estimates (Figure 6). MAR likely overestimates (solid) precipitation in this region which reduces melt (Fettweis et al., 2005), but microwave brightness temperatures could be biased by numerous rock outcrops (boulders) found in this mountainous region (Torinesi et al., 2003).

**Figure 6**

## 5. Runoff

[13] Mote (2003) uses a Positive Degree Day (PDD) model to deduce the runoff of the Greenland ice sheet from the satellite derived melt extent. Here we propose an estimation of the total ice sheet runoff coming from the melt extent surface detected by ImpXPGR. It is clear that ImpXPGR can not be used directly to quantify locally the runoff because it is based on a threshold value. Moreover, the runoff comes mainly from the low altitude regions along the ice sheet margin while ImpXPGR sometimes detects melt up to the crest of the ice sheet. However the more extended the melt area, the higher the melt takes place, the stronger the melt will be and will be the runoff. This hypothesis is confirmed in Figure 7 where a high correlation of 0.93 (resp. 0.84) is found between the 1990-2002 daily total ice sheet runoff simulated by MAR and the ImpXPGR (resp. XPGR) melt area. Based on this hypothesis and on the MAR results, an empirical estimation of the Greenland ice sheet runoff is made from the ImpXPGR melt extent via this linear regression:

$$Ru_{SSM/I} = ME_{SSM/I} \times 80.48\,10^{-7} - 0.19 \quad [2]$$

where $Ru_{SSM/I}$ is the total ice sheet runoff in km$^3$ yr$^{-1}$ and $ME_{SSM/I}$ is the melt extent in km$^2$ yr$^{-1}$ detected by ImpXPGR. The coefficients of the regression line are of course "model dependent". But, as far as we assume the linearity in this estimation to be correct, an increase of the melt extent (easily detected by satellite) corresponds to an increase of the ice sheet runoff in the same proportions, no matter the runoff value. The 1990-2002 RMSE between the MAR runoff and the ImpXPGR (resp. XPGR) derived runoff estimation is 0.53 (resp. 0.75) km$^3$. By comparison with Mote (2003) and Box et al. (2004) estimations, the runoff simulated by MAR (and then derived from SSM/I) is lower (see Figure 8), but it must be noted that the agreement with the satellite melt data is good.

[14] The linear relation has a negative intercept. ImpXPGR detects melt when the LWC of the top metre of snow is higher than 1 %. Before running off, a part of the meltwater is retained inside the snow pack assuming a maximum value for the LWC or can accumulate above ice or snow layers having high densities or being saturated by liquid water. The runoff of excessive internal and accumulated surface meltwater in MAR model is based on the work of Zuo and Oerlemans (1996) and described more in detail in Lefebre et al. (2003). The maximum value of the LWC is chosen to be 0.07 according to Colbeck (1974) and corresponds approximatively to a LWC of 3.5 % by volume in the top metre of snow that has a density of 500 kg/m$^3$ which is a typical value for a melting snow pack. Therefore, ImpXPGR detects the meltwater at the beginning of the ablation season before it can be run off in MAR, which explains the negative constant in the regression.

**Figure 7**

## 6. Melt trend estimates

[15] Between 1988 and 2003, XPGR and ImpXPGR respectively detect over the Greenland ice sheet an average increase of the cumulated melt extent of 0.2 % yr$^{-1}$ (+ 0.003×10$^7$ km$^2$ yr$^{-1}$) and of 1.7 % yr$^{-1}$ (+0.038 ×10$^7$ km$^2$ yr$^{-1}$) (Figure 8a). The cumulated melt extent is defined as the annual total sum of every daily ice sheet melt area. This trend corresponds to a melt area increase of respectively +0.049×10$^7$ km$^2$ and +0.581× 10$^7$ km$^2$ from 1988 to 2003 with a significance of about 85% for ImpXPGR. The signi-

ficance has been tested using a Monte-Carlo method with 1,000,000 simulations of autocorrelated data series with the same autocorrelation as the ImpXPGR time series. According to the previous section, we find this same trend in the total runoff of the ice sheet. The positive trend is higher with ImpXPGR because, as showing the ERA-40 reanalysis and MAR, rainfall on the ice sheet increases with temperature (Box, 2002). For the summers 1990-2002, MAR simulates an 0.20 °C $yr^{-1}$ increase of the mean air temperature above the ice sheet and an increase of the total rainfall on the ice sheet of 1.2 mm $yr^{-1}$. The trends of the mean melting area in June-July-August as defined by AS-1997 (Figure 8b) and of the maximum melting area as Steffen (2002) (Figure 8c) are also shown. But the cumulated melt area parameter is a better indicator of the total melt of the year.

**Figure 8**

[16] The melt zone extension lies mainly in the northern part of Greenland (especially the Humboldt Glacier) and along the western coast in the higher ablation zone and in the percolation zone (Figure 9). In the lower western ablation zone, no change is detected by the satellites because melt occurs already almost always during the melt season (see Figure 6). Except near Tunu in the percolation zone, the changes are very low along the eastern coast and the trend is even negative on the Greike Plateau. In this region, the trends (1990-2002) simulated by MAR are an increase of the snowfall, a decrease of rainfall and no temperature change which can explain the observed melt trends. Indeed, more snowfall and less rainfall decrease the LWC in the snow pack, raise the albedo and therefore reduce the melt. Finally, these regional trends are in agreement with AS2001 (see their Figure 3).

**Figure 9**

## 7. Conclusion

[17] A comparison between the Greenland melt extent simulated by the regional climate model MAR and derived from SSM/I satellite data has been performed. This has highlighted some biases during rainfall events in the XPGR algorithm (AS1997) used to retrieve melt area from passive microwave satellite data. The XPGR technique has been improved to correct the abnormally low satellite derived melt signals during rainfall

events. The agreement with the model has became clearly better. The improved XPGR method shows a cumulated melt area increase of 1.7 % $yr^{-1}$ ($+0.038 \times 10^7$ $km^2$ $yr^{-1}$) for the
312 period 1988-2003 (with a significance of about 85%). This increase is mainly situated in the North and along the West coast of Greenland in the ice sheet percolation zone. In the lower western ablation zone, no change is detected by the satellites because melt occurs
315 already almost always during the melt season. The non-modified XPGR technique shows a lower change because the rainfall on the ice sheet has also increased which partly masks the melt increase.

318 [18] Since 1988, the cumulated melt extent on Greenland has increased by almost 30 %. This trend agrees with recent observations highlighting rapid and substantial changes on the Greenland ice sheet due to a climate warming (Krabill et al. (2000), Rignot and
321 Thomas (2002), Schiermeier (2004)). Moreover, the melt of the Greenland ice cap may be irreversible (Toniazzo et al., 2004). By using model results, we have shown that the total Greenland ice sheet runoff is directly proportional to the melt extent detected by
324 the satellite. Therefore it is probable that the runoff has also increased in the same proportions which, combined to an ice discharge increase (Zwally et al., 2002) gives an increasing fresh water flux to the North-Atlantic ocean. These results are important for the
327 understanding of the effect of Greenland melting on the stability of the thermohaline circulation.

---

## 330 8. Acknowledgments

[19] Xavier Fettweis is a research fellow of the Belgian National Fund for Scientific Research. The authors acknowledge the National Snow and Ice Data Center (NSIDC,
333 Boulder, Colorado) for providing the passive microwave satellite data from SSM/I (see http://nsidc.org/). The authors acknowledge also Dr. Konrad Steffen for providing the GC-Net AWS measurements of 1998. The project was supported by the French pro-
336 gramme ACI-C3 (Ministère de la Recherche). All major computations were realized with IDRIS computing resources (France).

# 9. References

Abdalati W., and K. Steffen (1997) Snowmelt on the Greenland ice sheet as derived from passive microwave satellite data. *J. Climate*, 10, 165-175.

Abdalati W., and K. Steffen (2001) Greenland ice sheet melt extent: 1979-1999. *J. Geophys. Res.*, 106, 33983-3389.

Armstrong, R.L., K.W. Knowles, M.J. Brodzik and M.A. Hardman (1994) DMSP SSM/I Pathfinder daily EASE-Grid brightness temperatures, May to September 1990 & 1991. Boulder, CO: National Snow and Ice Data Center. Digital media and CD-ROM.

Box, J. E. (2002) Survey of Greenland instrumental temperature records: 1873-2001, *Int. J. of Climato., 22, 1829-1847.*

Box, J.E., D. H. Bromwich, L-S Bai, 2004: Greenland ice sheet surface mass balance for 1991-2000: application of Polar MM5 mesoscale model and in-situ data, *J. Geophys. Res.*, Vol. 109, No. D16, D16105, 10.1029/2003JD004451.

Colbeck, S. C. (1974) The capillary effects on water percolation in homogeneous snow, *J. Glaciol.*, 13(67), 85–97.

De Ridder, K., and H. Gallée (1998) Land surface-induced regional climate change in Southern Israel. *J. Appl. Meteorol.*, 37, 1470-1485.

Gallée, H. and G. Schayes (1994) Development of a three-dimensional meso-γ primitive equations model. *Mon. Wea. rev.*, 122, 671-685.

Gallée, H., G. Guyomarc'h and E. Brun (2001). Impact of the snow drift on the Antartic ice sheet surface mass balance: possible sensitivity to snow-surface properties. Boundary-Layer Meteorol., 99, 1-19.

Fettweis, X., Gallée, H., Lefebre, L., van Ypersele, J.-P. (2005) Greenland surface mass balance simulated by a regional climate model and comparison with satellite derived data in 1990-1991. *Climate Dynamics*, n° 24, 623-640, DOI: 10.1007/s00382-005-0010-y..

Krabill, W., Abdalati, W., Frederick, E., Manizade, S., Martin, C., Sonntag, J., Swift, R., Thomas, R., Wright, W. and J. Yungel (2000) Greenland Ice Sheet: High-Elevation Balance and Peripheral Thinning. *Science*, 289: 428-430.

Lefebre, F., H. Gallée, J. van Ypersele, and W. Greuell (2003) Modeling of snow and ice melt at ETH-camp (west Greenland): a study of surface albedo. *J. Geophys. Res.*, Vol. 108 No. D8, 10.1029/2001JD001160.

Lefebre, F., X. Fettweis, H. Gallée, J. van Ypersele, P. Marbaix, W. Greuell, and P. Calanca (2005) Evaluation of a high-resolution regional climate simulation over Greenland. *Climate Dynamics*, DOI: 10.1007/s00382-005-0005-8.

Mote, T. L. (2003) Estimation of runoff rates, mass balance, and elevation changes on the Greenland ice sheet from passive microwave observations. *J. Geophys. Res.*, 108(D2), 4056, doi :10.1029/2001JD002032.

Ohmura, A., K. Steffen, H. Blatter, W. Greuell, M. Rotach, M. Stober, T. Konzelmann, J. Forrer, A. Abe-Ouchi, D. Steiger, and G. Niederbaumer (1992) Energy and mass balance during the melt season at the equilibrium line altitude, Paakitsoq, Greenland ice sheet: Progress report 2, Dep. of Geography, Swiss Federal Institute of Technology, Zurich.

Rignot., E. and R. Thomas (2002) Mass Balance of Polar Ice Sheets. *Science*, 297, 1502-1506.

Schiermeier Q. (2004) Greenland's climate: A rising tide. *Nature*, 428, 114 – 115, doi:10.1038/428114a.

Steffen, K., and J. E. Box (2001), Surface climatology of the Greenland ice sheet: Greenland Climate Network 1995 – 1999, J. Geophys. Res., 106(D24), 33,951– 33,964.

Steffen, K. (2002) Greenland maximum melt extent available on http://cires.colorado.edu/steffen/melt/.

Steffen, K., S. V. Nghiem, R. Huff, and G. Neumann (2004) The melt anomaly of 2002 on the Greenland Ice Sheet from active and passive microwave satellite observations, *Geophys. Res. Lett.*, 31, L20402, doi:10.1029/2004GL020444.

Toniazzo, T., Gregory, J. M. and P. Huybrechts (2004) Climatic Impact of a Greenland Deglaciation and Its Possible Irreversibility. *Journal of Climate*, 17: 21-33.

Torinesi, O., M. Fily and C. Genthon (2003) Variability and trends of the summer melt period of Antarctic ice margin since 1980 from microwave sensors. *J. Climate*, 16, 1047-1060.

Zuo, Z., and J. Oerlemans (1996) Modelling albedo and specific balance of the Greenland ice sheet: calculations for the Sondre Stromfjord transect, *J.Glaciol.*, 42(141), 305–317.

Zwally, J.H., W. Abdalati, T. Herring, K. Larson, J. Saba, and K. Steffen (2002) Surface Melt-Induced Acceleration of Greenland Ice-Sheet Flow. *Science*, 297, 218-222.

Table 1. The 1990-2002 mean melt extent, correlation coefficient and Root Mean-Square Error (RMSE) between melt extent simulated by MAR and derived from SSM/I remote sensing observations by XPGR and ImpXPGR algorithms. According to Fettweis et al. (2005), MAR vs. XPGR "without rainfall/snowfall pixels" means that all the grid points with MAR daily liquid/solid precipitation greater than 1 mm/day have been not considered in the computation. The RMSEs and averages are expressed in percentage of the Greenland ice sheet area that lies in the intersection of both MAR and AS1997 ice mask (which covers 1.56 x $10^6$ km²).

| | ***MAR*** | ***XPGR*** | ***ImpXPGR*** |
|---|---|---|---|
| Mean melt extent | 8.73 % | 6.33% | 8.62% |
| Mean melt extent (without rainfall pixels) | 7.66% | 6.08% | 7.72% |
| Mean melt extent (without snowfall pixels) | 6.01% | 4.79% | 6.3% |
| Correlation coefficient with MAR | | 0.87 | 0.95 |
| Correlation coefficient with MAR (without rainfall pixels) | | 0.90 | 0.95 |
| Correlation coefficient with MAR (without snowfall pixels) | | 0.90 | 0.95 |
| RMSE with MAR | | 4.76 % | 2.56% |
| RMSE with MAR (without rainfall pixels) | | 3.64% | 2.44% |
| RMSE with MAR (without snowfall pixels) | | 3.04% | 2.10% |

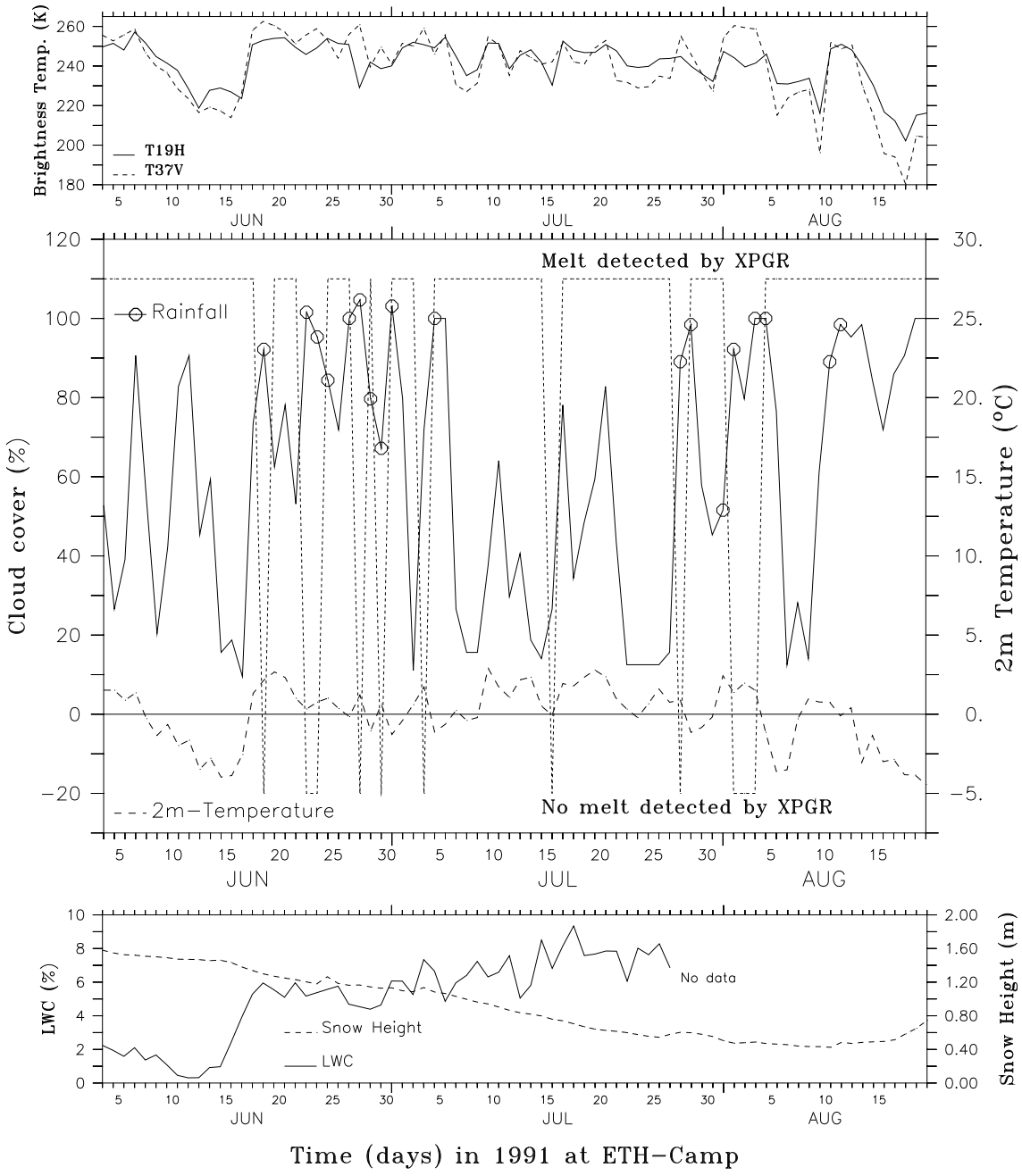


405 Figure 1. Top: the 19-GHz horizontal polarized brightness temperature (solid) and the 37-GHz vertical polarized brightness temperature (dashed) from SSM/I F-8 satellite at ETH-Camp. Middle: the daily means of the cloud cover (somlid) observed at ETH-
408 Camp. The circles on the curve indicate the days when rainfall was observed at ETH-Camp in 1991 (Ohmura et al., 1992). Also shown is the observed 2m-temperature (dashed) at ETH-Camp in 1991 (Ohmura et al., 1992). Finally, the dotted curve shows
411 when XPGR (AS1997) detects melt: above zero when XPGR detects melt, below zero otherwise. Below: the snow height (dashed) and its LWC (solid) observed at ETH-Camp. The ImpXPGR algorithm detects melt during the whole period (not shown). In
414 detail: improvement n°1 accounts for 11 days, improvement n°2 for 0 days, improvement n°3 for 0 days and improvement n°4 for 0 days.

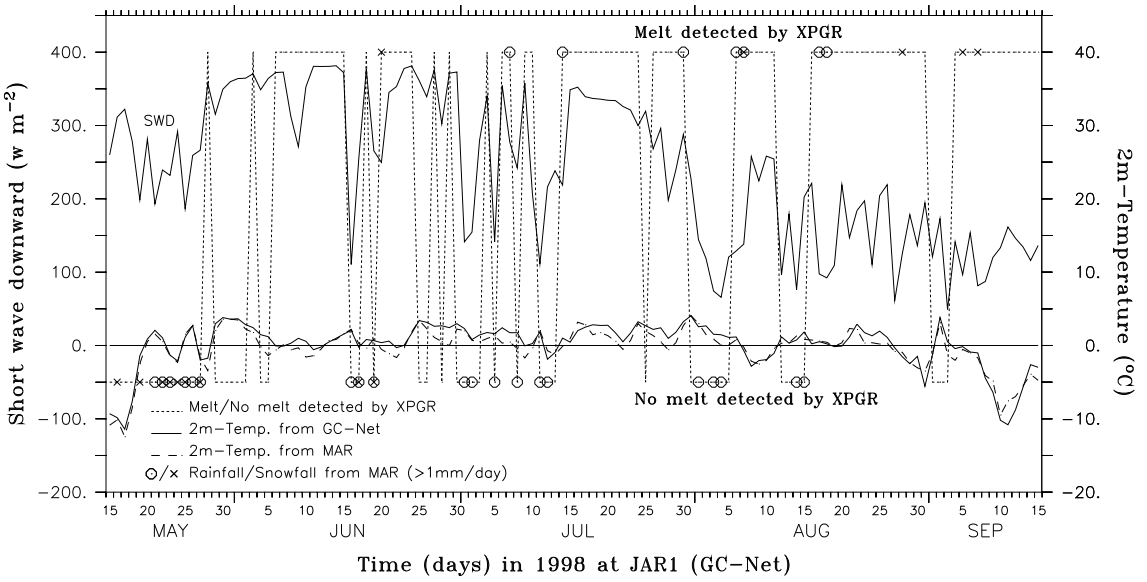


Figure 2. The solid lines show the daily means of the incoming shortwave (top, left axis) and the 2m-temperature (bottom, right axis) measured at the JAR1 AWS in the summer of 1998 (Steffen et al., 2001). The dotted curve shows when XPGR (AS1997) detects melt: above zero when XPGR detects melt, below zero otherwise. The 2m-temperature simulated by MAR is plotted with a dashed line. Days on which MAR simulates rainfall (resp. snowfall) higher than 1mm/day are indicated by circles (resp. crosses). Finally, the ImpXPGR algorithm and MAR detect melt continuously from May 22$^{th}$ to the end of September (not shown here). The ImpXPRG algorithm detects 42 more melt days than XPGR in 1998 at JAR1. In detail: improvement n°1 accounts for 34 days, improvement n°2 for 6 days, improvement n°3 for 2 days and improvement n°4 for 0 days.

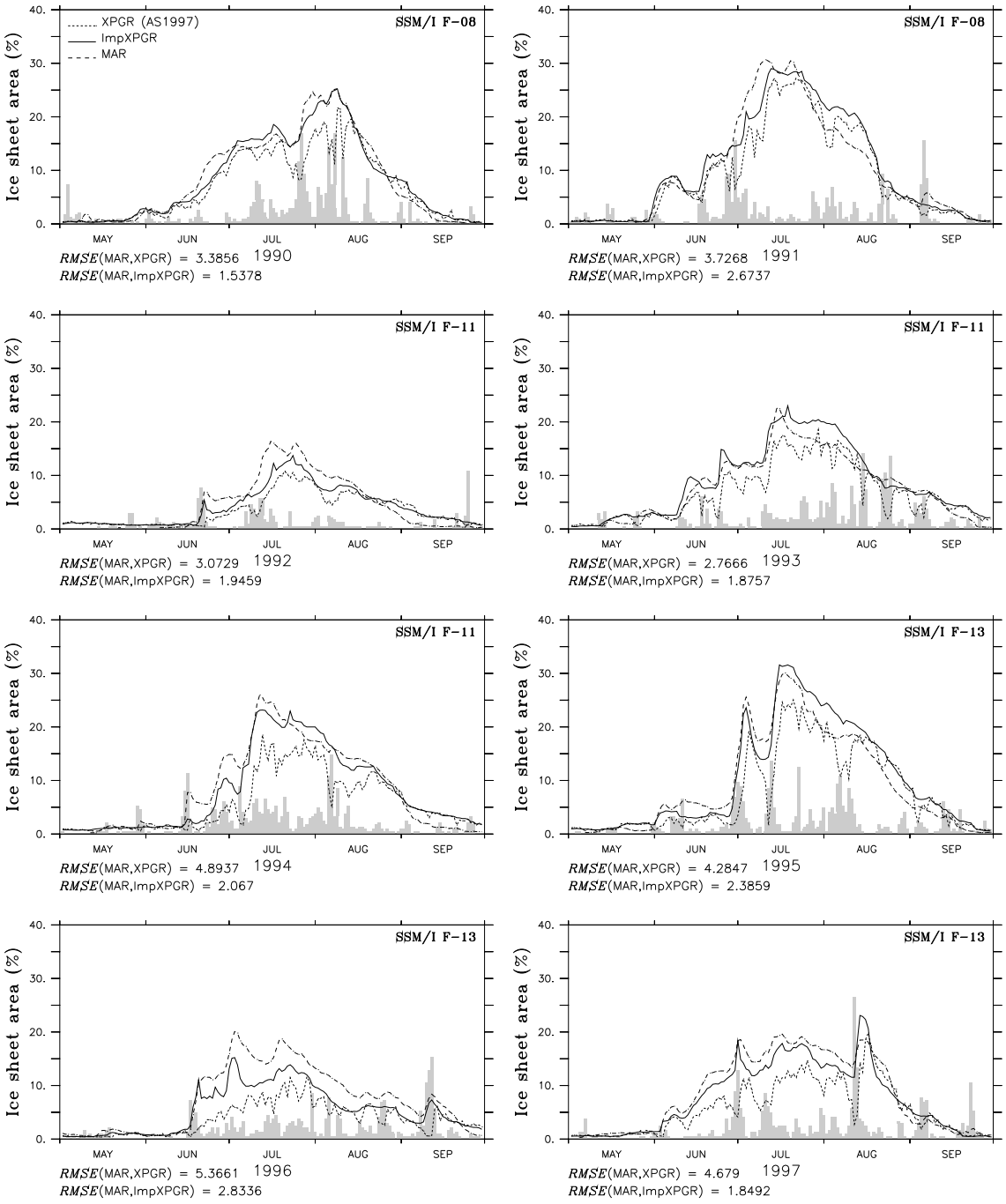


429 Figure 3. Daily mean melt zone extent detected by XPGR from AS1997 (dotted), by the improved XPGR (ImpXPGR) (solid) and simulated by MAR (dashed) for 1990-1997. Melt is expressed in percentage of the Greenland ice sheet area that lies in the
432 intersection of both MAR and AS1997 ice mask (which covers 1.56 x $10^6$ km²). Also shown is the percentage of Greenland ice sheet area where MAR simulates daily rainfall greater than 1 mm/day (grey bars).

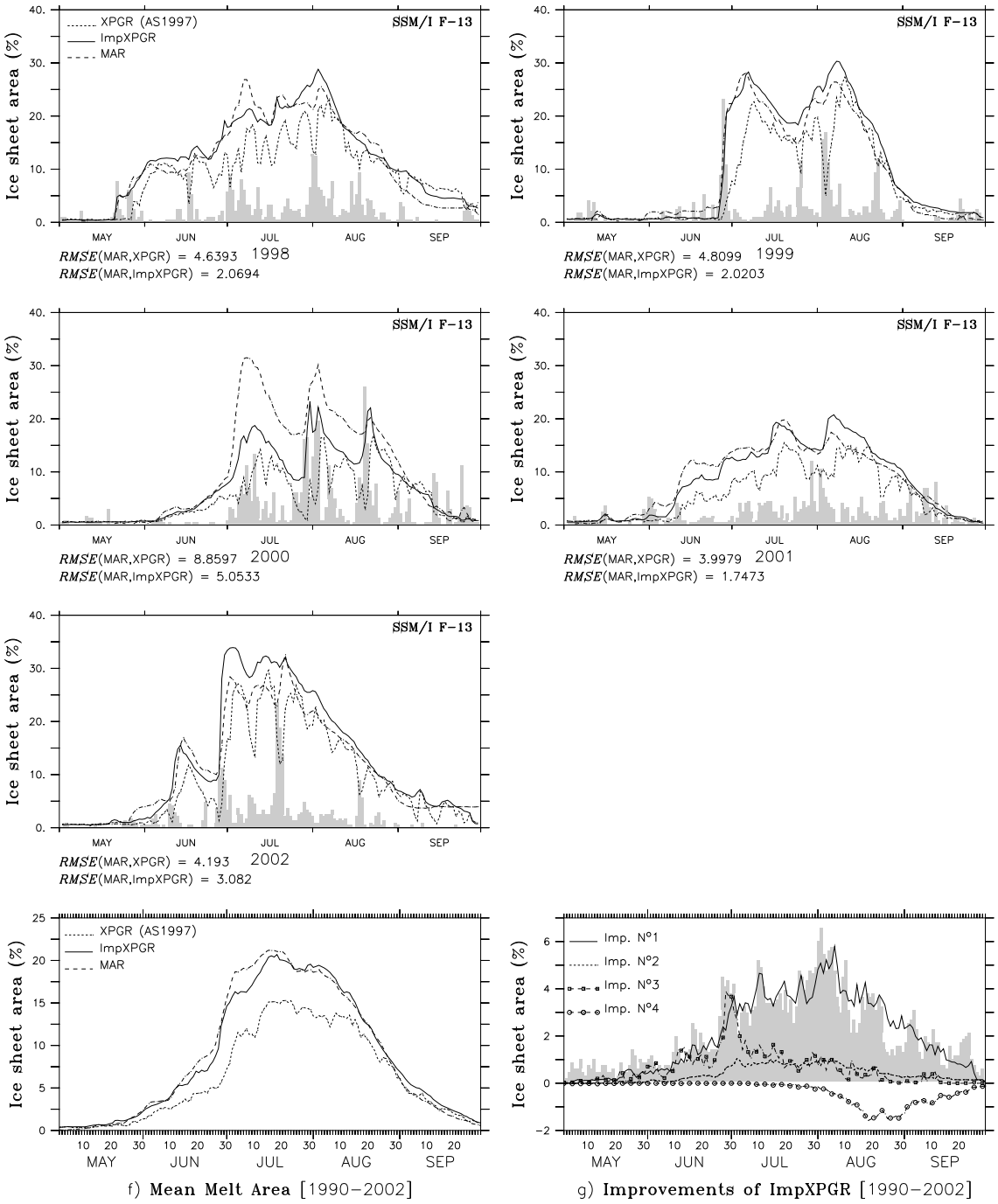


Figure 4. Same as Figure 3 but for 1998-2002. The last two plots (f and g) show the mean melt area for 1990-2002 and the mean relative effects of the four improvements of
438 ImpXPGR to the original XPGR algorithm (AS1997) presented in section 4.1. Also shown in g) is the 1990-2002 mean percentage of Greenland ice sheet area in which MAR simulates daily rainfall greater than 1 mm/day (grey bars). Note that the vertical
441 axis scales of the last two plots are different than before.

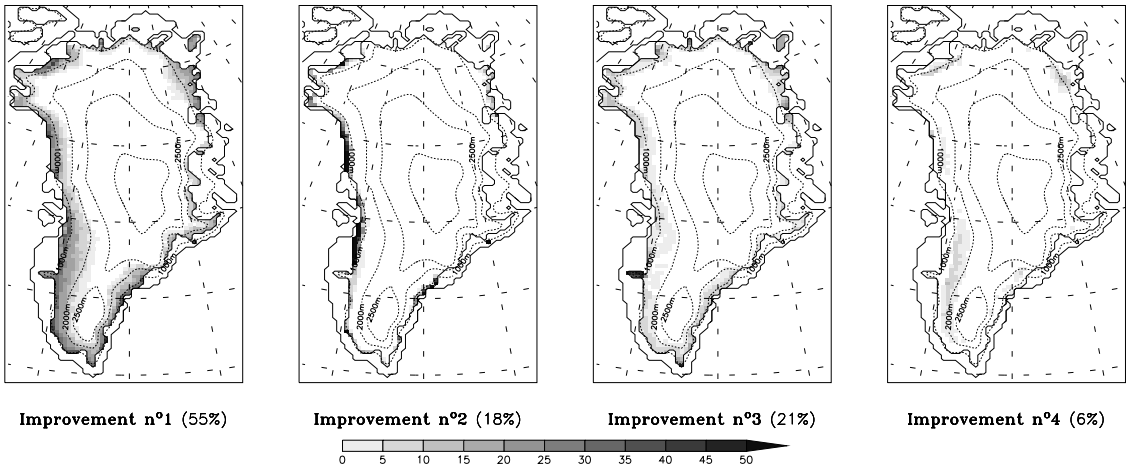


Figure 5. The number of ablation days per year, averaged over the 1990-2002 period, changed by the four corrections of ImpXPGR in comparison to the original XPGR algorithm detection. The first three improvements of ImpXPGR add melting days to original XPGR algorithm detection. The last one from which the absolute value is shown here removes melting days. The relative effect of each improvement is also indicated in brackets. Finally, this figure explains the differences between Figures 6.a and 6.b.

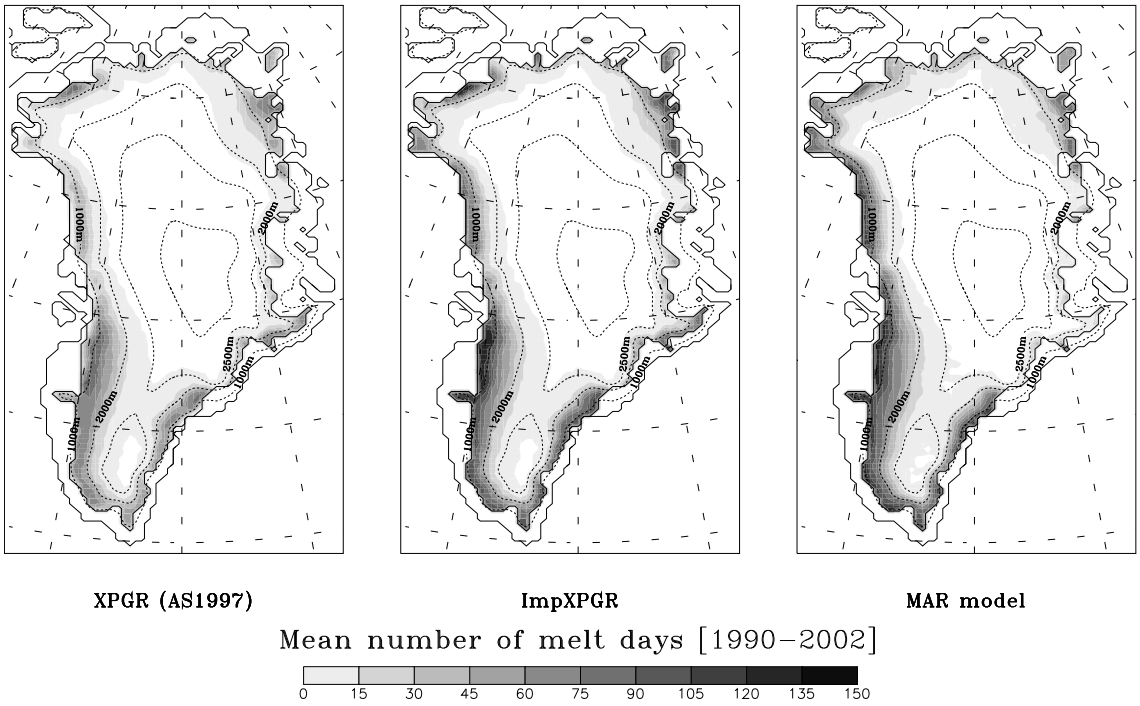


Figure 6. Yearly mean total number of ablation days detected by XPGR from AS1997 (left), by ImpXPGR (middle) and simulated by MAR (right).

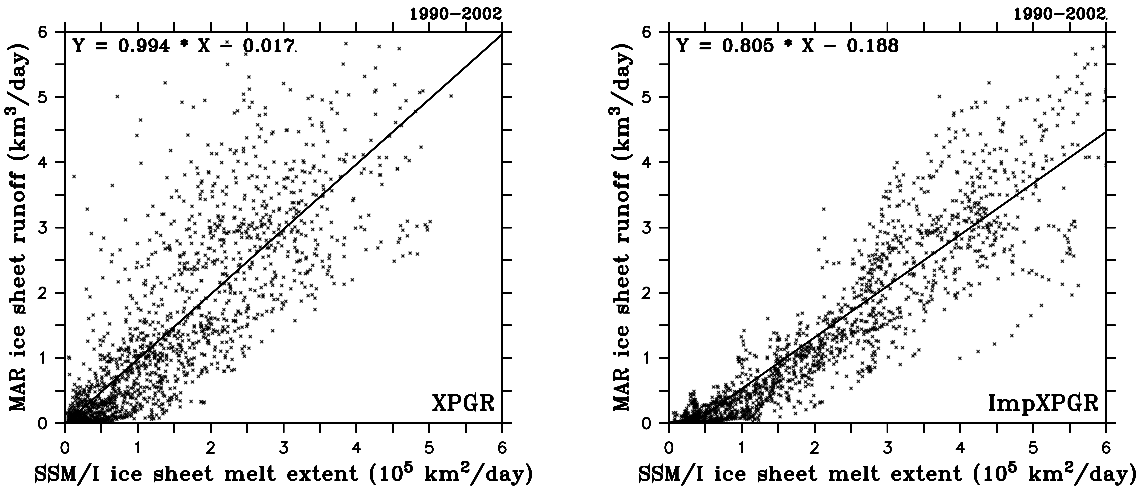


Figure 7. Comparison between the total ice sheet runoff simulated by MAR (in mm) and the melt extent detected by XPGR (left) and ImpXPGR (right) (in $10^5$ km$^2$) for the
456 period 1990-2002. The regression line is also plotted.

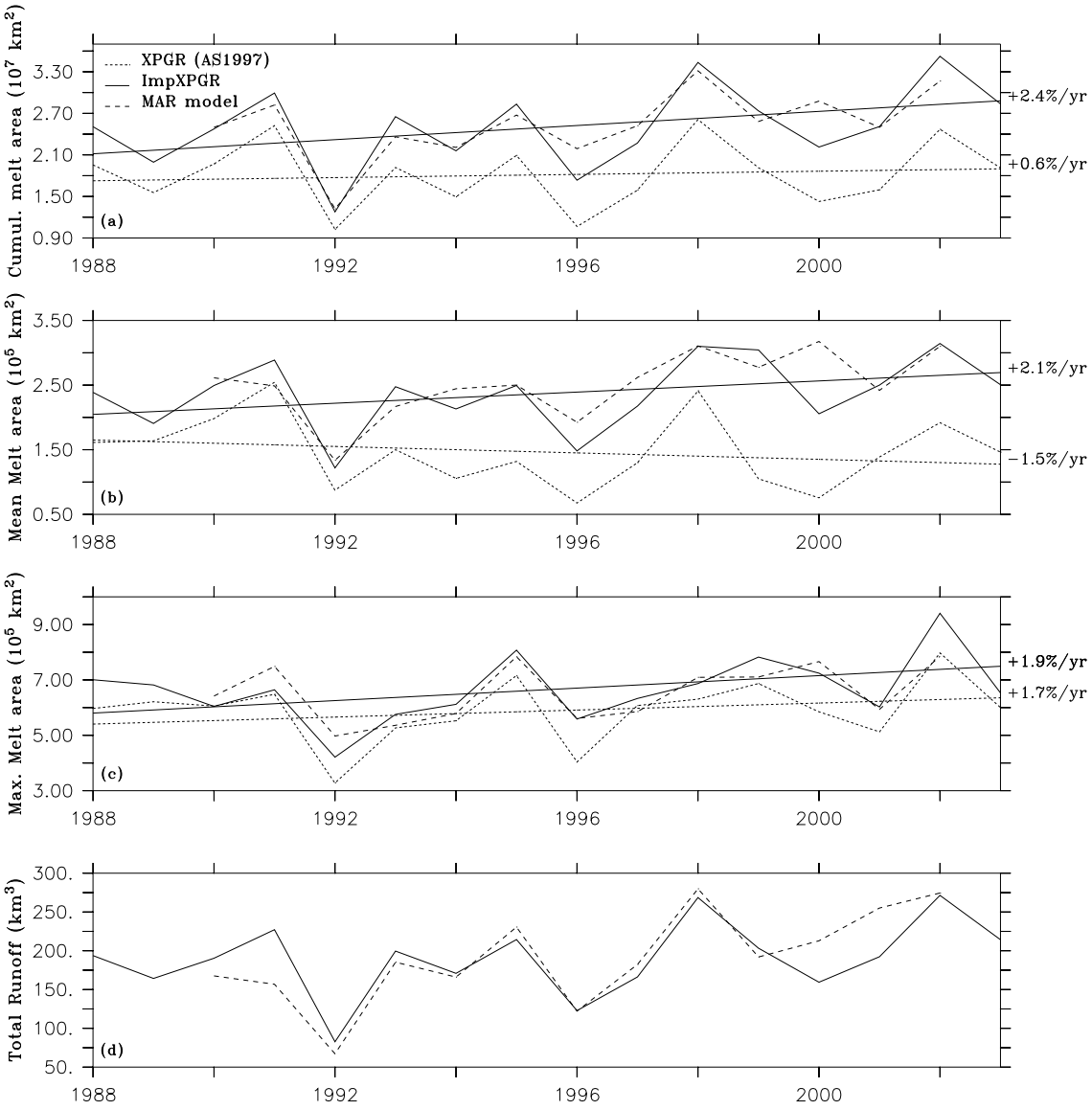


459 Figure 8. a) Annually cumulated melt area detected by XPGR from AS1997 (dotted), by ImpXPGR (solid) and simulated by MAR (dashed). b) Annually averaged summer mean melt extent defined by AS1997 (June, July, August). c) Maximum melt extent of the ice
462 sheet as in Steffen (2002). d) Total ice sheet runoff simulated by MAR and derived from the melt extent detected by ImpXPGR. The trends for XPGR (dotted) and ImpXPGR (solid) are also shown.

465

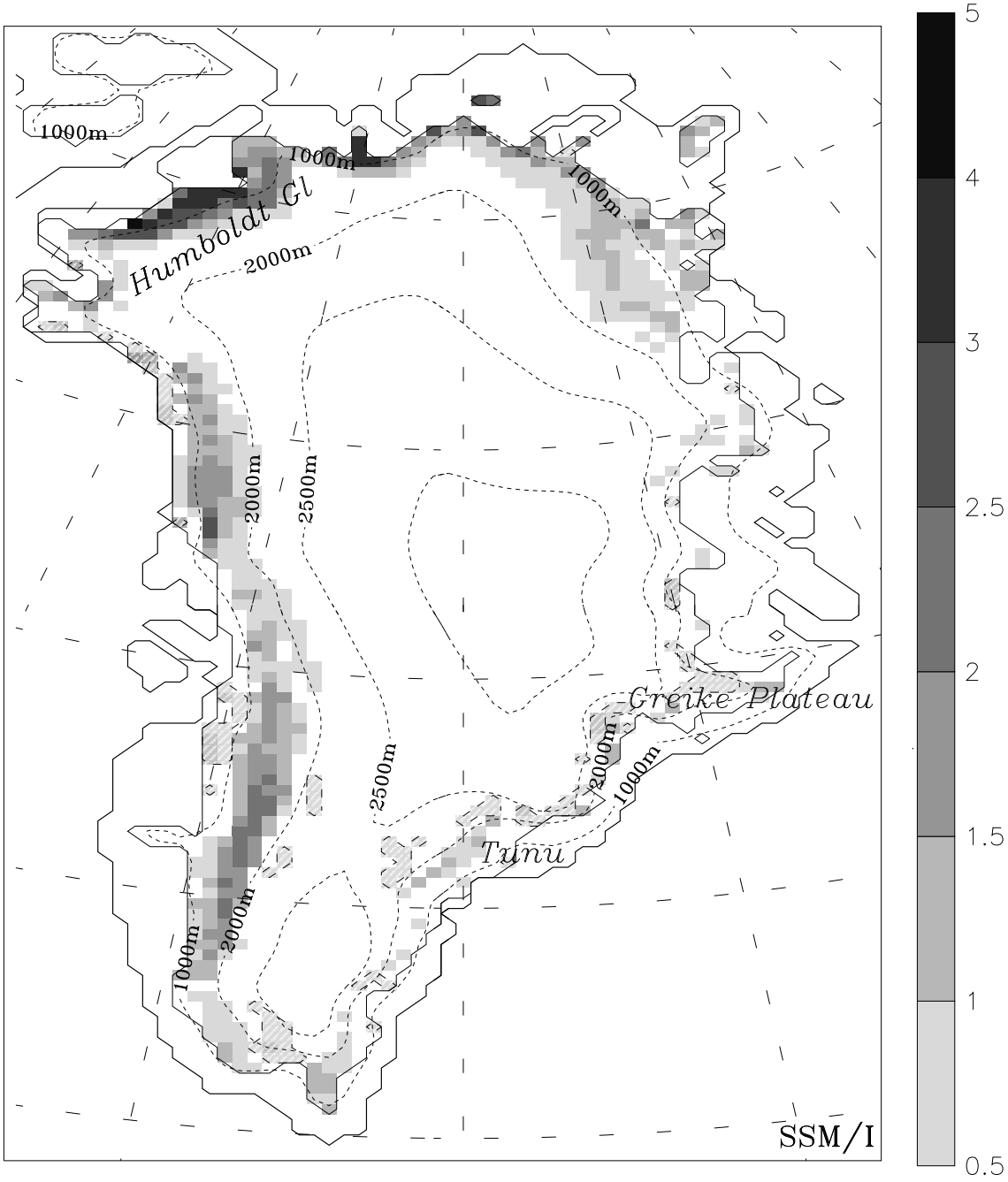


Figure 9. Melt trend in (ablation days) $(yr)^{-1}$ detected by ImpXPGR for the period 1988-
468 2003. Negative trends are hatched. This map shows also the locations (italic) quoted in the text.